Bi-layer in-situ Phosphorus Doped Poly-Si Films by PECVD for Blistering-free High-efficiency Industrial TOPCon Solar Cells

S. Ma[1,2], B. Liao[3,4*], D.X. Du[2], D. Ding[2], C. Gao[2], Z.P. Li[2], Q. Wang[3], X.Y. Wu[5], S. Zou[6], X. Su[6], R. J. Yeo[7], X. Li[4], W.M. Li[4], X.Y. Kong[1*], and W.Z. Shen[2*]

[1] School of Materials Science and Engineering, Shanghai Jiao Tong University, Shanghai 200240, People's Republic of China

[2] Institute of Solar Energy, and Key Laboratory of Artificial Structures and Quantum Control (Ministry of Education), School of Physics and Astronomy, Shanghai Jiao Tong University, Shanghai 200240, People's Republic of China

[3] School of Microelectronics and School of Integrated Circuits, Nantong University, Jiangsu 226019, People's Republic of China

[4] Jiangsu Leadmicro Nano-Equipment Technology Ltd., Wuxi, Jiangsu, 214028, People's Republic of China

[5] School of Photovoltaic and Renewable Energy Engineering, University of New South Wales, Sydney 2052, Australia

[6] School of Physical Science and Technology, and Jiangsu Key Laboratory of Thin Films, Soochow University, 1 Shizi Street, Suzhou 215006, People's Republic of China

[7] Institute of Materials Research and Engineering (IMRE), Agency for Science, Technology and Research (A*STAR), 2 Fusionopolis Way, Innovis #08-03, Singapore 138634, Republic of Singapore

[*]Corresponding author: wzshen@sjtu.edu.cn, xykong@sjtu.edu.cn, liaobaochen@ntu.edu.cn

Abstract:

The passivating contact concept stands out as one of the most promising and industrially viable photovoltaic (PV) technologies. Further improving the quality of physical contact has become a focus of ongoing research. The film blistering issue has been identified as one of the major bottlenecks for the polysilicon (poly-Si) films deposited by the PECVD approach. In this study, we investigated how the in-situ phosphorus (P) doping level within the poly-Si films contributes to the occurrence of blistering. Our investigations into the film blistering mechanisms reveal that a high in-situ P-doping suppresses hydrogen release levels and reduces the accumulation of residual stress during annealing, which leads to the blistering-free appearance, especially observed in heavily P-doped poly-Si films. However, as excessive P-doping could weaken the interfacial passivation quality, we propose a bi-layer structure of P-doped poly-Si films which allows the doping profile to be tailored and maintain good quality passivating contacts. Based on the bi-layer structure, we fabricated industrial-sized tunnel oxide passivated contact (TOPCon) solar cells, which attained an average efficiency of 23.84%. Our work not only presents a promising strategy for improving the

https://doi.org/10.1016/j.solmat.2024.112771.

performance of passivating contacts via the PECVD approach but also underscores the significant potential for its widespread implementation in industrial TOPCon solar cell manufacturing.

Keywords: Passivating contact, Film blistering, PECVD, In-situ phosphorus doping

1. Introduction

Tunnel oxide passivated contact (TOPCon) solar cells have gained widespread acceptance among mainstream industrial solar cell manufacturers owing to their passivating contact structure, which effectively reduces carrier recombination loss at the cell's rear-side metal contact [1, 2]. Typically, the superior surface and chemical passivation effects of the passivating contact structure in TOPCon cells are attributed to the presence of a heavily doped poly-Si layer and a very thin tunnel SiO_x layer (generally 1.4-1.5 nm), respectively [3, 4], which results in low recombination current density (J_0) of < 5 fA/cm^2 and low contact resistivity (ρ_c) of < 10 mΩ cm^2 [5, 6]. Recently, fabricated TOPCon solar cells have achieved record power conversion efficiencies (PCEs) of 25.8% on *n*-type *c*-Si [7], 26.0% on *p*-type *c*-Si [8], and 26.1% on IBC [9] solar cells. These values are close to the theoretical PCE of 28.7% calculated for a bi-facial TOPCon solar cell [10]. Poly-Si films can be fabricated by various methods, including plasma-enhanced chemical vapor deposition (PECVD) [11-15], low-pressure chemical vapor deposition (LPCVD) [16-19], atmospheric-pressure chemical vapor deposition (APCVD) [20], hot-wire chemical vapor deposition (HWCVD) [21], and physical vapor deposition (PVD) [22-25], with each method presenting its unique characteristics. Based on cost and performance considerations, the industry predominantly adopts two methods: PECVD and LPCVD. Presently, LPCVD edges out PECVD as the preferred method of choice in the industry due to the more mature technology of LPCVD. Nevertheless, in comparison to LPCVD, the PECVD method possesses desirable qualities such as higher thin film deposition rates, minimal wrap-around deposition, and reduced consumption of equipment-related consumables [26]. Consequently, tube-PECVD technology, which is capable of integrating the tunnel SiO_x and in-situ doped poly-Si deposition processes, has significant potential for industrial mass-production of TOPCon solar cells [27].

Doped poly-Si deposited through PECVD followed by a thermal annealing process for crystallization presents an alternative route that detours drawbacks compared to the LPCVD approach. However, the a-Si film deposited by PECVD is susceptible to poor passivated contacts while the blistering phenomenon occurs in the film during the subsequent annealing process, both of which lead to a significant degradation in device performance [28]. The crystallization of a-Si films induces interfacial stress accumulation and rapid hydrogen (H) release, identified as the primary contributors to the blistering phenomenon [29, 30]. Several strategies have been proposed to mitigate this issue. One common strategy involves implementing slow thermal processing to gradually release hydrogen during annealing, thus preventing its excessive accumulation at the film/SiO_x interface [31]. Another strategy is to change either the temperature, reduce the H_2/SiH_4 flow ratio, or use Ar instead of H_2 to control the film's H content or porosity [31-34]. Additionally, modifying the surface topography and adjusting the poly-Si thickness have been identified as beneficial for suppressing blistering [35]. However, one of the most successful strategies in preventing blistering is to incorporate the elements of carbon (C), nitrogen (N), and oxygen (O) into the poly-Si film during deposition [36-39]. Lin et al. [36] investigated doping poly-Si film with C and attributed the reduced crystallization fraction of poly-Si along with the inhibited level of

https://doi.org/10.1016/j.solmat.2024.112771.

hydrogen release to the suppression of blistering. Similarly, Yang et al. [37] fabricated N-incorporated Si films without film blistering, also linking this to the reduction of poly-Si crystallization. Zhou et al. [38] studied O-incorporated Si films, achieving blistering-free films with moderate O doping. Finally, Sharma et al. [39] compared different PECVD-grown Si-rich amorphous films doped with adequate amounts of C, N, or O, and then demonstrated that the absence of blistering was due to the low intrinsic stress in the films. They concluded that O-incorporated films were the most suitable for SiO_x-based passivating contacts due to their high excess Si content and crystallization. Although incorporating small molecule elements like C, N, and O can solve the issue of blistering, a side-effect of this doping causes the conductivity of the poly-Si film to decline, which greatly affects the electrical performance of the cells. Therefore, maintaining a blistering-free PECVD-grown poly-Si film while ensuring the performance of cells has become a focus of research on industrial TOPCon solar cell fabrication.

In this work, we present a simple, effective, and industrially viable method utilizing the PECVD technique to implement in-situ P-doping poly-Si films, thereby addressing the concerns of blistering while also imparting high electrical conductivity within the poly-Si film as required by TOPCon solar cell applications. Investigations into blistering mechanisms indicated that in-situ doped P could suppress hydrogen release levels and reduce residual stress during annealing, primarily accounting for the blistering-free appearance of P-doped poly-Si films. Furthermore, we propose a bi-layer structure of P-doped poly-Si, i.e., the inner layer adjacent to SiO_x is lightly P-doped and the remaining outer layer is heavily P-doped, with the goal of tailoring the doping profile within the poly-Si film, and further enhancing the passivation contact quality. Observations of surface morphology revealed the absence of blistering for the bi-layer structure of poly-Si film, with subsequent passivation and contact tests confirming the optimal performance. Finally, we fabricated industrial-sized TOPCon solar cells based on the bi-layer structure with 800 pieces of 182 × 182 mm^2 Si wafers, achieving an average efficiency of 23.84%, which is 0.26% higher than that of heavily P-doped poly-Si counterparts (23.58%). The results of this work underscore the tremendous potential of our developed in-situ P-doped PECVD poly-Si film with a bi-layer structure for the industrial manufacturing of high-efficiency TOPCon solar cells.

2. Experimental methods

To evaluate the performance of P-doped poly-Si films, we fabricated the rear passivation layers on the industrial Czochralski (Cz) *n*-type silicon wafers with a size of 182 x 182 mm^2 (M10), thickness of 150 ± 20 μm, and resistivity of 0.3-2.1 Ω·cm. Appropriate characterizations were performed on the polished wafer to investigate the film's performance. The polished wafer mentioned in this work was fabricated as follow: the *n*-Si substrate was first cleaned and textured, and then polished by alkaline solution. The surface morphology of polished wafer used in our experiment was consistent with the actual rear-side of TOPCon on the production line, which made our work more practical and meaningful.

2.1. Fabrication of PECVD P-doped poly-Si films

Fig. 1 illustrates the manufacturing process involved in fabricating the rear passivated contact structure for TOPCon solar cells. Before the deposition of the passivation layers, the polished wafer underwent RCA cleaning to eliminate contaminants. The tube-PECVD (*ZR5000, Leadmicro*) with

a direct radio frequency (RF) plasma source operating at 40 kHz was used to sequentially deposit both the interfacial ultrathin SiO_x and in-situ P-doped a-Si. The deposition was conducted at 400 °C with different precursor gases (SiO_x: N_2O; P-doped a-Si: PH_3, SiH_4, H_2, respectively). In this work, to facilitate the comparison of the effect of different P-doping levels in poly-Si, the same thickness of SiO_x was used in all samples by fixing the SiO_x deposition time at 3 min. Different P-doping levels in a-Si were achieved by separately setting the flow rates of PH_3 at 0 sccm, 500 sccm, 2000 sccm, and 3500 sccm to obtain undoped, lightly doped, moderately doped, and heavily doped a-Si, respectively, corresponding to the respective sample groups of Baseline, G1, G2, and G3. The thickness of poly-Si for all groups was set to 140 nm. Following that, an annealing process was carried out under nitrogen (N_2) atmosphere (*XH10000A, Leadmicro*) at a temperature of 900 °C for 45 min to transform a-Si to poly-Si and simultaneously activate the dopants. Lastly, a hydrogenation step was executed by depositing a 70 nm SiN_x capping layer via PECVD at 450 °C (*PD-405C, S.C.*).

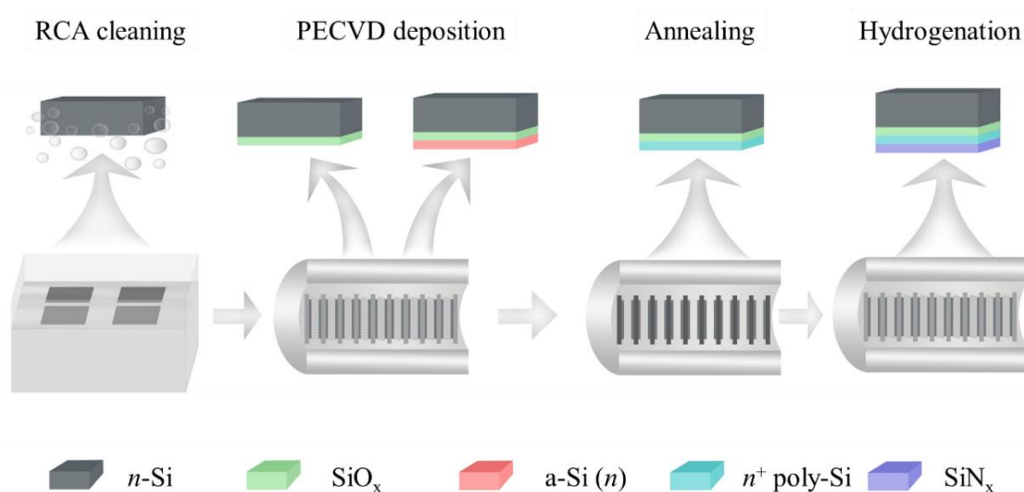

Fig. 1. Fabrication process for n^+ poly-Si/SiO_x/*c*-Si contacts, beginning with RCA cleaning and followed by PECVD deposition of tunneling oxide and P-doped a-Si, annealing, and hydrogenation.

2.2. Fabrication of TOPCon cells

To investigate the film's performance at the device level, the manufacturing process of TOPCon cells underwent the following steps on the production line as shown in Fig. 2(b): (1) The *n*-type wafers were first saw-damage etched (SDE) in potassium hydroxide (KOH) then subjected to an alkaline texturing on both sides of the wafer, resulting in a pyramid size of ~2 μm. After cleaning, boron diffusion was performed in a tube furnace using boron trichloride (BCl_3) as a dopant source to form a p^+ layer. Subsequently, an inline single-side etch (SSE) was performed to remove the wrap-around p^+ doping, and then the rear surface was polished by alkaline solution; (2) the SiO_x and in-situ phosphorus-doped a-Si: were deposited by the tube PECVD (*ZR5000, LeadMicro*); (3) the annealing process was carried out under N_2 atmosphere (*XH10000A, Leadmicro*) at the temperature of 900 °C for 45 min, and the edge wrap-round deposition of poly-Si was removed with hot KOH solution; (4) the front side was capped by a 3 nm thickness of AlO_x with tube-ALD (*Leadmicro*) and the both sides were deposited a 70 nm thickness of SiN_x with tube-PECVD (*PD-405C, S.C.*) sequentially; (5) the electrode pattern was fabricated by screen printing (*Softline-DL-SP, Maxwell*) Ag-Al paste on the front and Ag paste on the rear, followed by belt-furnace firing

https://doi.org/10.1016/j.solmat.2024.112771.

(*CFSeries, Despatch*) to form the metal contacts and activate H atoms.

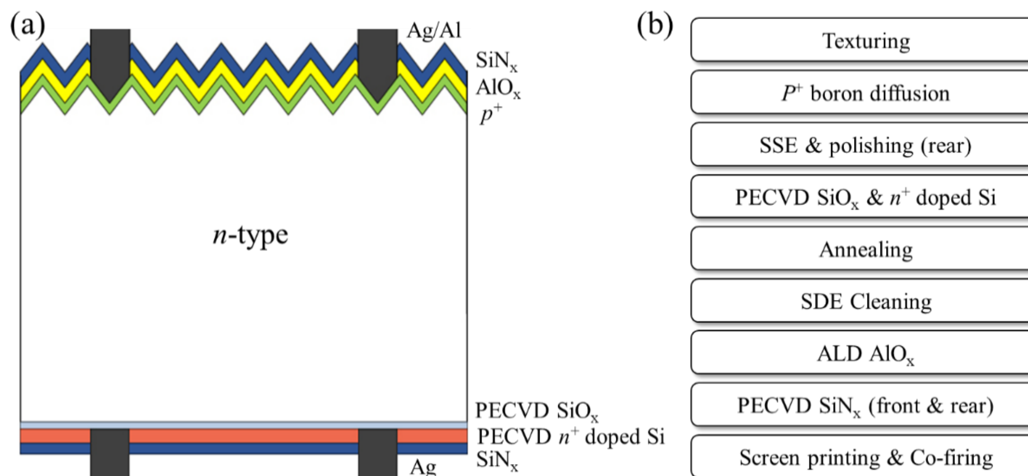

Fig. 2. (a) Schematic of *n*-type TOPCon cells and (b) the fabrication process on the production line.

2.3 Characterizations

X-ray photoelectron spectroscopy (XPS, *Axis Ultra DLD*) was performed to investigate the effects of the different doping levels within poly-Si films on the chemical bonding states of the Si-P. The refractive index (n) and extinction coefficient (k) of different poly-Si films were measured by spectroscopic ellipsometry (SE). X-ray diffraction (XRD, *ARL Equinox 3500*) was used to characterize the crystallographic phases of poly-Si with different doping levels. The surface morphology of the samples was investigated by optical microscope (OM, *Leica DM 4000*) and scanning electron microscope (SEM, *Jeol JSM-7800F*). Fourier transform infrared spectroscopy (FTIR, *Bruker Vertex 70*) was used to analyze the chemical bonding in the deposited films. The active dopant was characterized by electrochemical capacitance-voltage profiling (ECV, *WEP CVP21*). Samples with symmetrical structures were prepared to investigate the effective minority carrier lifetime (τ_{eff}), which was measured by a quasi-steady-state photo conductance method (*Sinton Instruments WCT-120*) at an injection density of 1 x 10^{15} cm^{-3}. The single-side J_0 was determined according to the high-injection method proposed by Kane and Swanson [40]:

$$\frac{1}{\tau_{eff}} - \frac{1}{\tau_{Auger}} = \frac{1}{\tau_{SRH}} + \frac{2J_0(N_d+\Delta n)}{q\, n_i W}$$

where τ_{eff}: the measured effective carrier lifetime of the sample, τ_{Auger}: the intrinsic Auger lifetime [41], τ_{SRH}: the defect-related Shockley-Read-Hall bulk lifetime, N_d: the bulk doping concentration, Δn: the excess carrier density, q: the elementary charge, n_i: the intrinsic carrier concentration, and W: the sample thickness. The contact resistivity (ρ_c) was measured by the transfer length method (TLM, *Ai-shine*). The electrical parameters of TOPCon solar cells were measured by *Halm 3600* under standard test conditions (AM 1.5G spectrum, 25 °C).

3. Results and discussion

Examination of the changes in chemical bonding states is crucial for discussing dopant pile-up and redistribution in the near-surface region of the poly-Si films after annealing. In this study, XPS analysis was employed to investigate the chemical bonding states in poly-Si films with different P-

https://doi.org/10.1016/j.solmat.2024.112771.

doping levels. In Fig. 3(a), the XPS survey scans of poly-Si films revealed peaks corresponding to Si 2s, Si 2p, O 1s, and C 1s, which was consistent with previous reports [42]. Fig. 3(b) presents a magnified image of the binding energy range of 50-200 eV, where a closer view of the peaks in this region could be visualized. The P 2p peak position of ~129 eV as expected in the literature is indicated in the figure [42]. To explore the chemical characteristics of P 2p bonding in the P-doped films, we performed high-resolution XPS scans focusing on the P 2p core level region. For a quantitative analysis, curve fitting of the high-resolution P 2p spectra was performed using Gaussian-Lorentzian components after Shirley-type background subtraction. The fitted spectra were divided into three well-resolved contributions (plasmon loss peak of Si 2p, P $2p_{1/2}$, and P $2p_{3/2}$) as depicted in Fig. 3(c)-(f). The broad peak located at 134.0 eV for all samples is primarily attributed to the plasmon loss peak of Si 2p photoelectrons, but could also have a minor contribution from P-O bonding [43]. The constituent peaks at binding energies of 129.9 and 129.0 eV are attributed to the P $2p_{1/2}$ and P $2p_{3/2}$ components of P bonded with Si, respectively [44, 45]. These two corresponding peaks have an area ratio of 1:2, and the spin-orbit splitting between them was 0.90-0.95 eV, with reasonable full width at half maximum (FWHM) values of less than 1.0 eV, which was in good accordance with the literature value of 0.99 eV [46]. Without P-doping in poly-Si (Fig. 3(c)), the corresponding P $2p_{1/2}$ and P $2p_{3/2}$ peaks did not appear, as the intensity of the single peak corresponding to Si-P bonding was not strong enough to be split into P $2p_{1/2}$ and P $2p_{3/2}$ peaks, consistent with previous findings [47]. As the P-doping concentration increased, the P $2p_{1/2}$ and P $2p_{3/2}$ peaks appeared and their intensities increased accordingly as expected. These results demonstrate that the P atoms are incorporated into the silicon lattices during PECVD in situ P-doping poly-Si. The experimental observations by XPS serve as clear evidence of the incorporation of P into Si lattices after PECVD in-situ doping and demonstrate the increase of Si-P bonds with the augmentation of the PH_3 flow rate.

https://doi.org/10.1016/j.solmat.2024.112771.

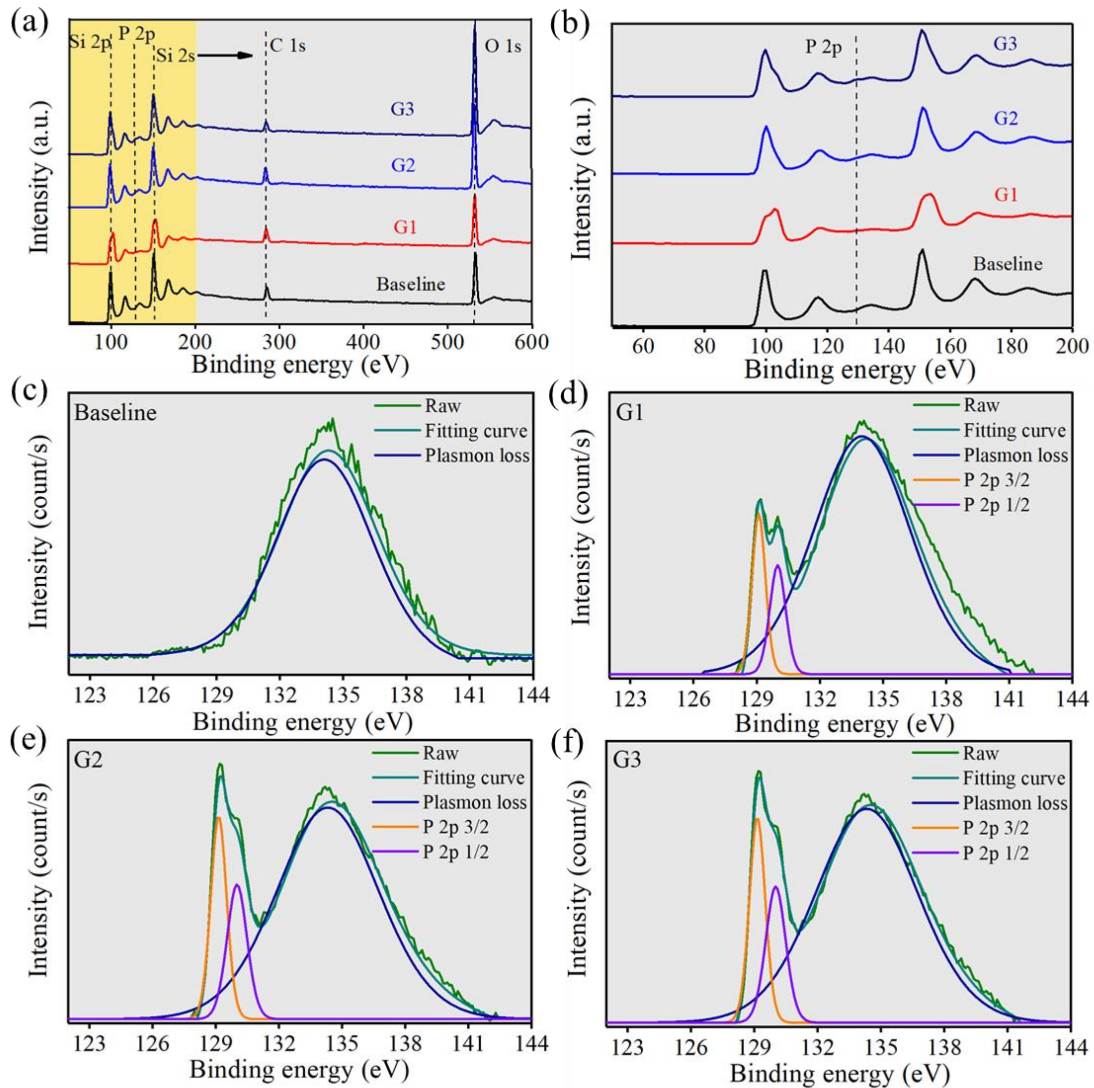

Fig. 3. (a) Full-range XPS spectra and (b) the magnified image of the P 2p core-level region for poly-Si films with different P-doping levels. (c)-(f) Deconvoluted P 2p spectra of (c) Baseline, (d) G1, (e) G2, and (f) G3. Undoped, lightly doped, moderately doped, and heavily doped a-Si samples are denoted as Baseline, G1, G2, and G3, respectively.

Due to the narrow band gaps and considerable absorption coefficients of materials utilized in existing passivating contact structures, such as a-Si and poly-Si, significant parasitic absorption losses may be introduced compared to other *c*-Si/Si alloys with equivalent thickness but a larger band gap. These optical losses are particularly significant in poly-Si films, hence limiting their use in the passivating contact structure. Therefore, the study of the optical loss of these films is very important as well. With the aid of spectroscopic ellipsometry, the refractive index (n) and optical extinction coefficient (k) of different groups of samples in the wavelength range of 300-1000 nm can be extracted, as shown in Fig. 4(a) and Fig. 4(b), respectively. Since the poly-Si films are commonly used on the rear surface of TOPCon solar cells, their optical performance in the long wavelength range of 600-1000 nm is particularly critical. The long wavelength n and k values of Baseline and G1 had little difference, indicating that the lightly P-doped poly-Si did not significantly reduce the parasitic absorption of the film. When the doping concentration increased to the moderate

https://doi.org/10.1016/j.solmat.2024.112771.

level (G2), the corresponding n and k values increased at the long wavelength range, revealing that the parasitic absorption of the poly-Si film layer could decrease above a certain level of P-doping concentration. Compared to the G2 group, heavy P-doping (G3) could further reduce the parasitic absorption of the film. To further investigate the effect of P-doping on the optical absorption of the poly-Si film, we input the n and k values from ellipsometry into OPAL2 simulations to calculate the reduction in the current density (ΔJ_{SC}) absorbed in the films, as shown in Fig. 4(c). For different P-doping concentrations, the parasitic absorptions in a device-relevant stack of air/poly-Si (140 nm)/*c*-Si on a textured wafer were computed. The equivalent ΔJ_{SC} was then measured by integrating the product of absorption and photon flux (standard AM 1.5 G spectrum) within the wavelength range of 600-1000 nm. From this method, we obtained a potential total J_{SC} reduction of up to 5.11 mA/cm^2 (600-1000 nm) for the heavily P-doped poly-Si film (G3). The above results verified that when the P-doping concentration exceeds a certain level, the parasitic absorption of the poly-Si film starts to decrease. The XRD patterns of the films are presented in Fig. 4(d). Three main Si peaks are observed, corresponding to the orientations of (111), (220), and (311), respectively. The well-known reflections of the crystalline poly-Si film along the (111), (220), and (311) orientations were obtained at 2θ = 28.4°, 47.3°, and 56.2°, respectively [48-50], whereas the forbidden peak for Si (002) at 2θ = 33.1° was reported to arise due to multiple diffractions [51]. The XRD spectra clearly showed that the intensities of the main three diffraction peaks were simultaneously enhanced with the increase in the P-doping level in the poly-Si film. This result suggests that P-doping could increase the crystallinity of a-Si during annealing, which is related to the passivation effect of the poly-Si film.

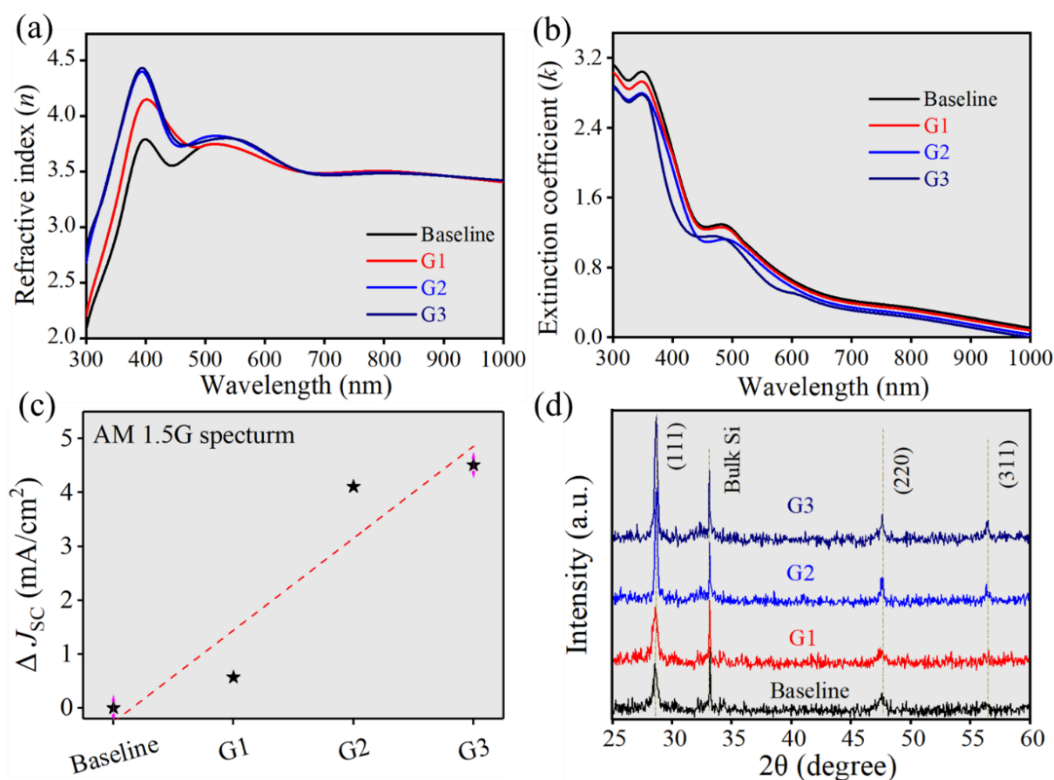

Fig. 4. Refractive index (a) and extinction coefficient (b) of samples extracted by spectroscopic ellipsometry as a function of wavelength. (c) Calculated reduction in current density absorbed in the P-doped poly-Si films based on OPAL2 simulations. (d) XRD patterns for the P-doped poly-Si

https://doi.org/10.1016/j.solmat.2024.112771.

samples showing the crystallographic peaks corresponding to the (111), (220), (311) orientations and bulk Si (002). The Baseline, G1, G2, and G3 samples correspond to undoped, lightly doped, moderately doped, and heavily doped poly-Si, respectively.

The issue of film blistering poses a significant challenge in the manufacturing of TOPCon devices, particularly when utilizing the PECVD method. It is widely recognized that the occurrence of blistering is primarily attributed to hydrogen-rich precursor gases and the conditions of deposition. The "hydrogenated" a-Si thin film releases its hydrogen content of 10^{20}~10^{22} cm^{-3} during high-temperature annealing [29]. At the interface between a-Si and SiO_x, a portion of the released hydrogen accumulates, ultimately leading to the formation of blisters. Additionally, the presence of a thin SiO_x layer between the Si substrate and poly-Si film in the passivating contact structure contributes to the poor adhesion of the SiO_x layer with the Si substrate or poly-Si film, resulting in the blistering phenomenon as observed on the polished *c*-Si surface. The underlying mechanism can be attributed to the difference in the thermal expansion coefficients between the SiO_x layer and poly-Si film, leading to the accumulation of residual stress after thermal annealing [32]. Due to the inhomogeneity of the film morphology and the elongation of the lateral transport channel, blisters form, significantly diminishing the TOPCon device performance [52]. In this study, the SiO_x/poly-Si passivation layer was prepared on the rear side of the polished *c*-Si substrate with varying P-doping levels corresponding to the Baseline, G1, G2, and G3 samples. To examine the poly-Si surface morphology of the samples after annealing, OM and SEM were employed to observe the surfaces of the samples at magnifications of 800× and 1500×, respectively, as displayed in Fig. 5(a). From the images, it is evident that the surface of the Baseline sample exhibited severe film blistering after annealing. However, when poly-Si was lightly P-doped (G1), film blistering only appeared in localized areas. With a gradual increase in P-doping, film blistering on the poly-Si surface was no longer observed. These observations demonstrate that film blistering can be significantly suppressed by in-situ P-doping poly-Si via the tube PECVD method, and can be eliminated beyond a certain P-doping level.

To investigate the microstructural details and elucidate the blistering-free behavior of P-doped poly-Si films, Raman spectroscopy studies were conducted. As depicted in Fig. 5(b), the Raman intensity of the characteristic Si peak at 520 cm^{-1}, indicative of the crystalline fraction of poly-Si films, gradually increased with the increase in P-doping concentration. The crystallinity was determined by the integrated area ratio of grain boundary and crystalline phases relative to the total area of the three peaks [53]. Specifically, the crystallization fractions were found to be 78.2%, 80.6%, 85.6%, and 85.2% for the undoped, lightly doped, moderately doped, and heavily doped samples, respectively. These results indicate that the introduction of P effectively enhances the crystallization of poly-Si films, consistent with the earlier XRD findings. Furthermore, with an increase in P-doping concentration, the local Raman peak at 520 cm^{-1} gradually shifted towards higher wavenumbers as shown in Fig. 5(c), suggesting the release of tensile stresses in the poly-Si films. For the undoped sample, a relatively higher tensile stress of 600.3 MPa was extracted from Raman spectra [54], decreasing to 448.1, 300.4, and 295.6 MPa for the lightly, moderately, and heavily P-doped samples, respectively, as shown in Fig. 5(d). When the residual stress surpasses the fracture strength of the material, blistering occurs to release some of this residual stress, resulting in a lower apparent stress value extracted from Raman measurements [36]. These results collectively demonstrate that in-situ P-doped poly-Si grown using the tube-PECVD method can significantly

https://doi.org/10.1016/j.solmat.2024.112771.

enhance the crystalline fraction of poly-Si and reduce the residual stress of the film, ultimately suppressing the occurrence of film blistering.

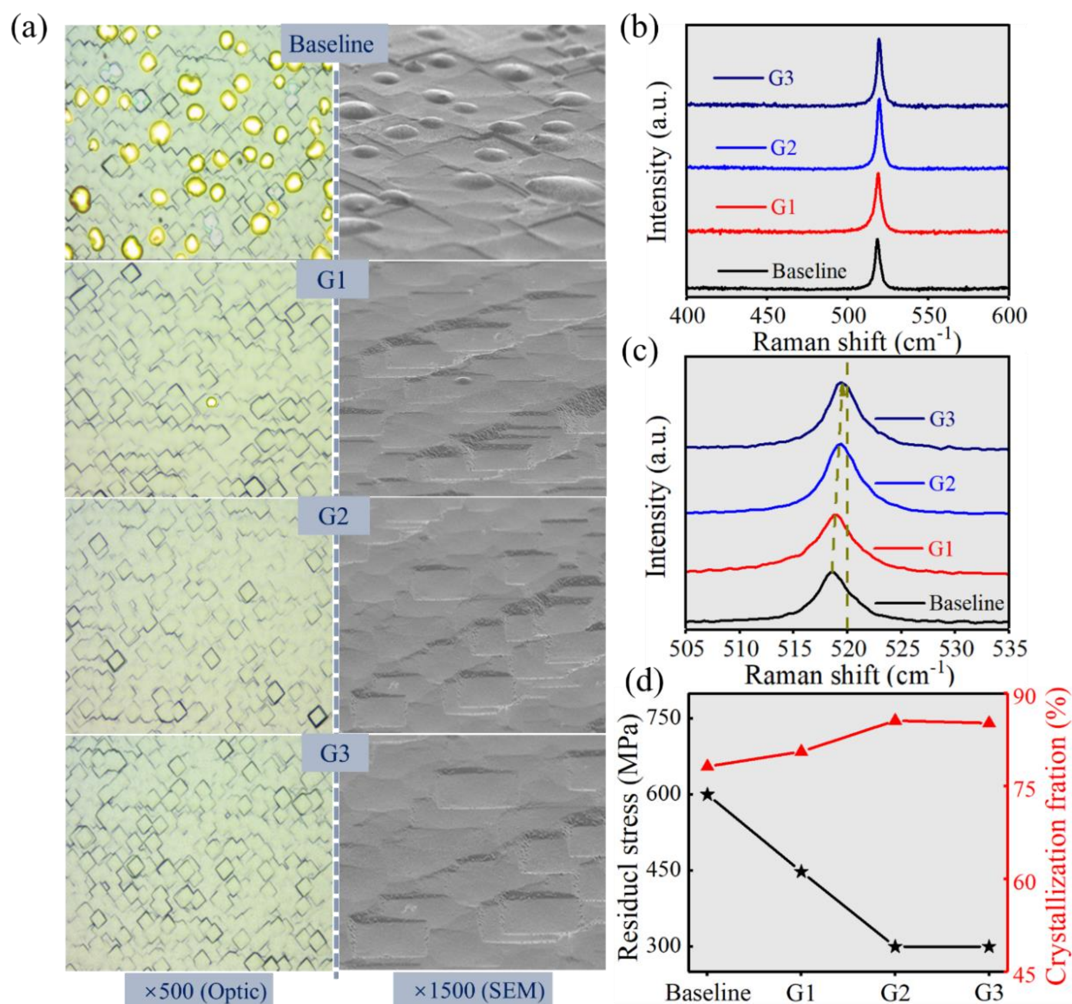

Fig. 5. (a) OM photographs and SEM images of the samples after annealing. (b) and (c) Raman spectra under different Raman shift ranges. (d) Distributions of crystallization fractions and residual stresses for the four related samples extracted from Raman intensity and shift. Baseline, G1, G2, and G3 samples correspond to undoped, lightly doped, moderately doped, and heavily doped poly-Si, respectively.

As reported in the existing literature, the blistering phenomenon observed in poly-Si films is intricately linked to the escape of H atoms during the annealing process. Nuclear magnetic resonance (NMR) experiments in literature have indicated that molecular hydrogen constitutes up to 40% of the overall hydrogen content in a-Si [55]. To explore the characteristics associated with Si-H bonding, FTIR was conducted on the poly-Si films with different P-doping levels (Fig. 6(a)). The absorption bands in the FTIR spectra corresponding to Si-H bonds were prominent at 650 cm^{-1} and 1940-2120 cm^{-1}, corresponding to the wagging and stretching Si-H modes, respectively [56, 57]. The hydrogen content of the material was ascertained by performing a peak integration of the wagging-mode band at 650 cm^{-1}, which can be used as a measure of the total hydrogen content independent of any bonding configurations [56, 57]. Furthermore, the heavily P-doped poly-Si film exhibited a more pronounced Si-H wagging mode at 650 cm^{-1}. This observation signifies an increase

https://doi.org/10.1016/j.solmat.2024.112771.

in bonded H, which mitigates the release of H atoms during annealing, and consequently diminishes the likelihood of film blistering. This finding is in concordance with the trends observed in Fig. 5(a). The interplay between ionic energy transfer and unbonded H at a low PH_3 gas flow rate resulted in energy-activated H diffusion to the interface of a-Si/*c*-Si. This process also saturated any dangling bonds at the interface, thereby reducing the density of interface-trapped charges (D_{it}). The effusion of hydrogen is influenced by both the hydrogen content and the material's microstructure [36]. Consequently, the stretching mode observed at 1940–2120 cm^{-1} in the FTIR spectra is significant. Through the deconvolution of this band, various bonding configurations, including monohydride, dihydride, and multi-hydride configurations, could be analyzed [58]. The close-up view of the Si-H, Si-H_2, and (Si-H_2)$_n$ stretching modes in Fig. 6(b) provides a clearer view of these stretching modes. The stretching modes can be divided into two regions, namely the low stretching mode (LSM) region at around 1940 cm^{-1} and the high stretching mode (HSM) region at approximately 2120 cm^{-1}. In Fig. 6(c), the microstructural parameter, R*, for different poly-Si films was calculated. The R* value, determined by the ratio of the peak area corresponding to the HSM to the total peak area of the stretching mode contribution (LSM+HSM), serves as a quantifier of the microstructural quality of the films and an indicator of nanovoid concentration [34]. An elevated R* value implies that the poly-Si film is porous with a less organized network structure, where hydrogen atoms exist in the form of SiH_2 and $(SiH_2)_n$ bonds. On the other hand, a lower R* value suggests a more compact structure dominated by Si-H bonds [59]. Notably, with higher P-doping, the R* value increased, indicating higher film porosity and more hydrogen being trapped as SiH_2 and $(SiH_2)_n$ bonds at the molecular level, which is counterproductive to film blistering. This trend aligns with unexpected findings reported in earlier studies [36]. In summary, a P-rich poly-Si film effectively captured more H atoms, which was in favor of mitigating the occurrence of film blistering during the annealing process. Additionally, the captured hydrogen contributed to enhanced surface chemical passivation of the passivation layer, thereby reducing recombination losses.

https://doi.org/10.1016/j.solmat.2024.112771.

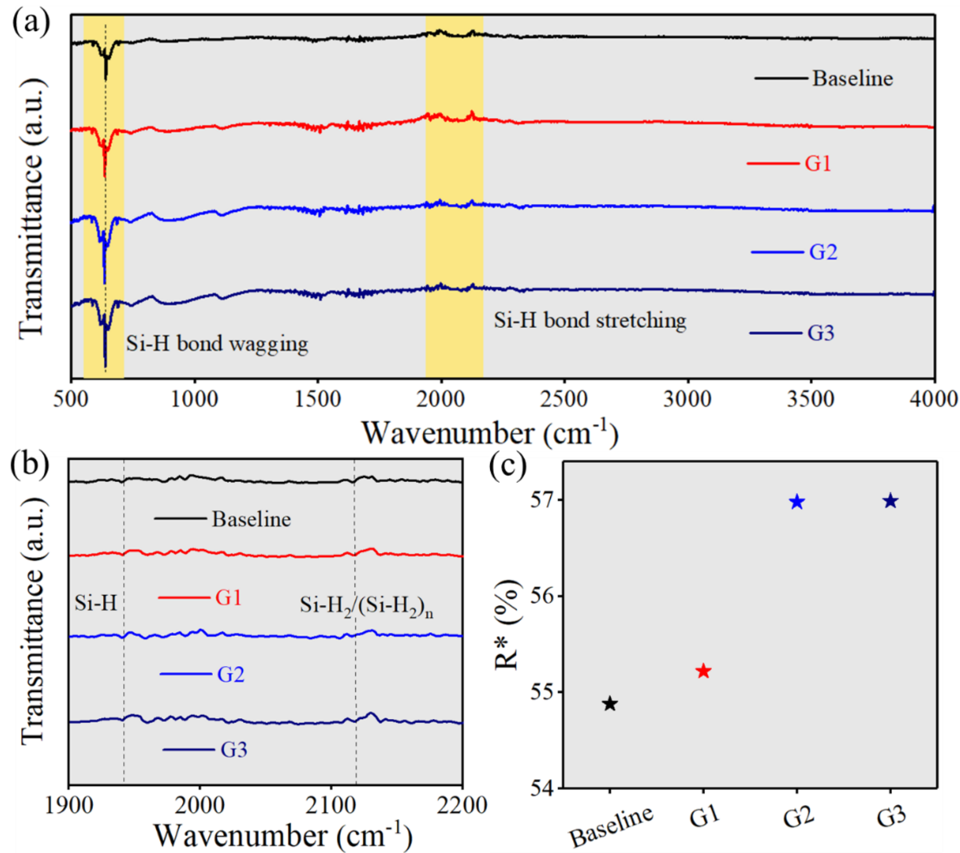

Fig. 6. (a) FTIR measurements of doped poly-Si films with different P-doping levels, with the yellow vertical bands indicating the regions of interest corresponding to the wagging and stretching modes of Si-H bonds. (b) A magnification of the spectra focusing on the region of interest corresponding to the Si-H and Si-H_2/(SiH_2)$_n$ stretching modes. (c) Microstructure factors (R*) of doped poly-Si films with different P-doping levels. Baseline, G1, G2, and G3 samples correspond to undoped, lightly doped, moderately doped, and heavily doped poly-Si, respectively.

During the annealing process, dopants within the heavily doped poly-Si film can diffuse into the *c*-Si substrate, forming a buried dopant region (called in-diffusion dopant) near the *c*-Si interface. Although the existence of in-diffusion dopants is beneficial for metal contact to a certain extent which reduces contact resistance, however, the presence of excessive amounts of dopants could severely weaken the interfacial passivation quality. To control dopant diffusion into the Si substrate and attain an optimal equilibrium, it is essential to precisely manage and optimize the dopant concentration within the poly-Si film after the annealing process. Therefore, we proposed a bi-layer structure of doped poly-Si films denoted as sample G4, i.e., the inner layer (~ 30 nm) adjacent to SiO_x was lightly P-doped, and the remaining outer layer (~110 nm) was heavily P-doped as shown in Fig. 7(a). Herein, we adopted this bi-layer structure of P-doped poly-Si, aiming to ensure sufficient field passivation effect through the use of heavily doped poly-Si, while reducing the recombination loss caused by P diffusion to the substrate through the use of the lightly doped poly-Si layer. Before discussing the bi-layer structure, we observed its surface morphology through OM and SEM. We found that this bi-layer structure did not undergo film blistering after annealing as shown in Fig. 7(b). Compared with the blistering situation of lightly doped poly-Si in sample G1 shown in Fig. 5(a), the results proved that the bi-layer structure was much less prone to film

https://doi.org/10.1016/j.solmat.2024.112771.

blistering even with the incorporation of a thin ~30 nm lightly doped poly-Si layer.

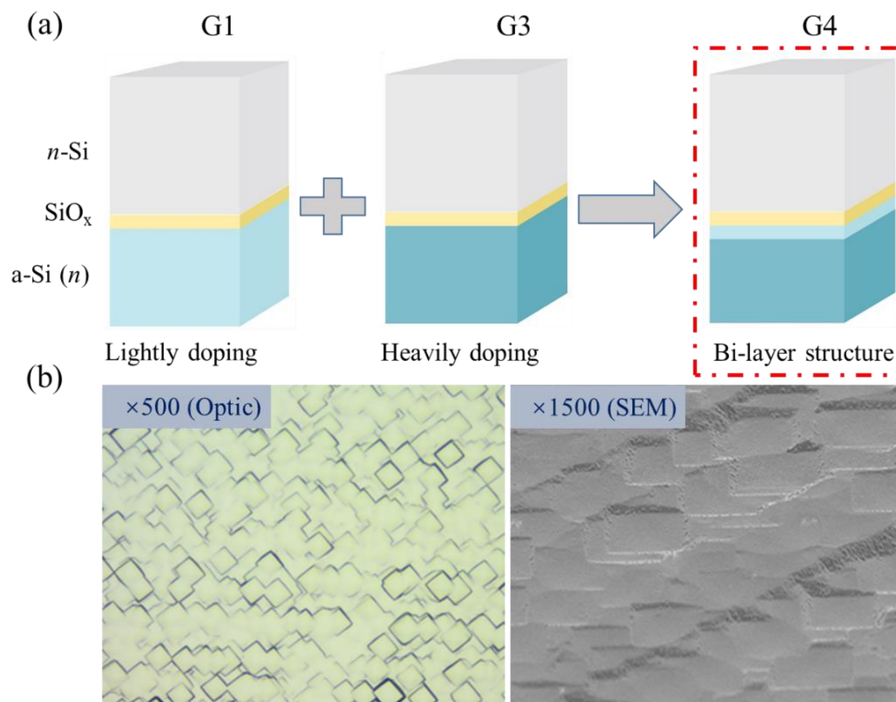

Fig. 7. (a) Schematic illustration of the bi-layer structure of P-doped poly-Si (sample G4). (b) Surface morphology of sample G4 after annealing as confirmed by OM and SEM.

To evaluate the impact of poly-Si with different P-doping levels on the TOPCon solar cell performance, characterizations were conducted on the rear passivation layer. Firstly, we used the ECV method to measure the concentration of active P as shown in Fig. 8(a). It can be seen that the concentration of active P within poly-Si was close to 10^{21} cm^{-3} for samples G2, G3, and G4, whereas the active P concentration was close to 10^{20} cm^{-3} for sample G1, indicating that the P-doping improved with the increase of PH_3 flow rate. Compared with sample G2, sample G3 exhibited a similar C-V curve, revealing that when the flow rate of PH_3 was increased beyond a certain extent, the doping concentration no longer increased at higher PH_3 flow rates. These above observations were consistent with the XPS and XRD results. The C-V curve analysis revealed that the decline in the P concentration across the SiO_x layer for G4 was steeper than that of samples G2 and G3, suggesting that there was a more pronounced blocking effect by the bi-layer structure on P diffusion, i.e., fewer P atoms could diffuse into the *c*-Si substrate. The aforementioned observations substantiated our conclusion that the doping profile can be controlled via the bi-layer structure design of P-doped poly-Si. In the etch depth range of 0.18-0.22 μm, the P concentration increased slightly due to the annealing process. The P concentration of this section is important for the subsequent metallization, which significantly impacts the performance of the final TOPCon solar cell device. To gain deeper insights into the rear passivation layer's performance with different P-doping levels, further investigations were conducted on the passivation and contact properties of the TOPCon solar cells. Fig. 8(b) illustrates the symmetrical structure (I) used for testing the iV_{OC}, J_0, and carrier lifetime. Additionally, the semi-manufactured structure (II) presented in the figure was designed for measuring the contact resistivity (ρ_c) using the TLM. The corresponding results of passivation and contact properties are displayed in Fig. 8(c) and Fig. 8(d), respectively. As seen

https://doi.org/10.1016/j.solmat.2024.112771.

from Fig. 8(c), when the P-doping was increased from G1 to G3, the corresponding iV_{OC} and carrier lifetime increased from 704.5 mV to 726.1 mV and from 618 μs to 1028 μs, respectively, whereas the J_0 decreased from 19.9 fA/cm^2 to 11.1 fA/cm^2. This implied that the passivation performance of the samples improved with increasing P-doping. The reason for the improvement in passivation performance could be attributed to the enhanced field passivation of poly-Si with the increase of the P-doping level. When the bi-layer structure of the poly-Si film was adopted, the corresponding iV_{OC} increased further to 736.8 mV, demonstrating that the bi-layer structure of P-doped poly-Si had an analogous blocking effect on P diffusion compared to other samples, which was in alignment with the ECV results. In Fig. 8(d), the contact performance of the passivation layer with different P-doping levels was measured by the TLM. A schematic illustrating the top view of the samples used for TLM measurements is presented in the figure (III). When poly-Si was lightly P-doped (G1), the corresponding contact resistivity reached 28.2 mΩ cm^2, which was significantly higher than that of the other samples, mainly due to its low P-doping concentration as shown in Fig. 8(a). In contrast, the contact resistivity of G4 had a similar value to the G2 and G3 samples, revealing that the contact performance was not affected by the introduction of the bi-layer structure. Considering both the passivation and contact performance, it was established that the TOPCon solar cells achieved optimal performance with the implementation of the bi-layer structure. These research outcomes underscore the significance of the bi-layer structure design for P-doped poly-Si, which effectively retards the diffusion of P into the Si substrate, leading to enhanced passivation effects. This strategic addition further allows for the possibility of fine-tuning the doping profile, ultimately contributing to the development of high-efficiency solar cells.

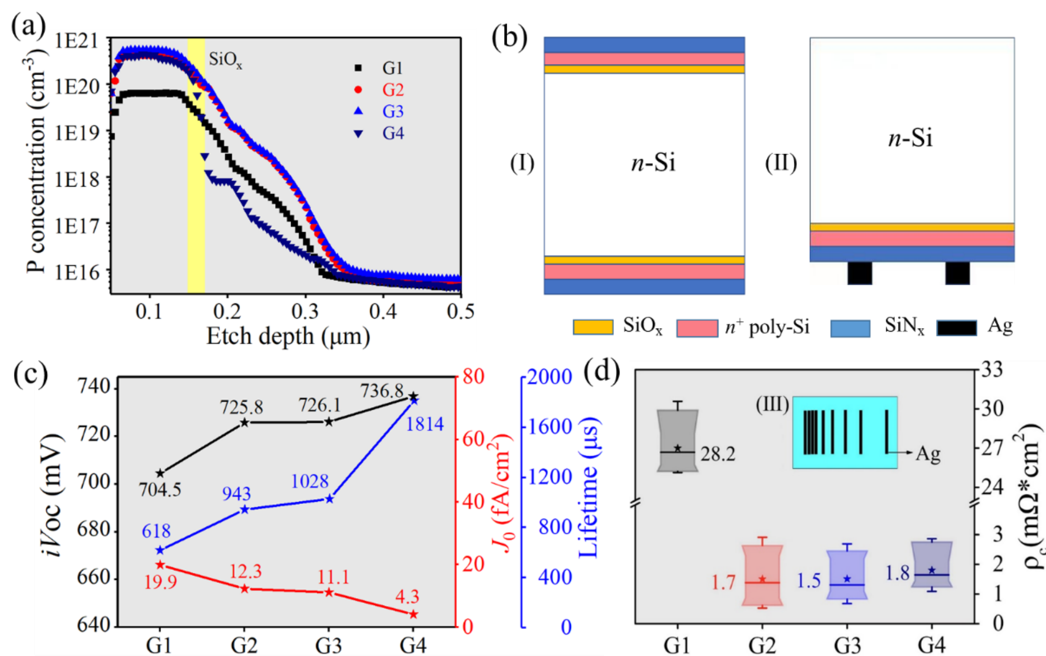

Fig. 8. (a) Active P concentration of the samples measured by ECV. (b) Schematic illustrations of the symmetrical structure used to test iV_{OC}, J_0, and carrier lifetime (I), and the semi-manufactured structure designed to measure contact resistivity (ρ_c) by the TLM (II). (c) Measured iV_{OC}, J_0, and carrier lifetime values extracted from the symmetrical test samples. (d) Contact resistivity (ρ_c) measured by the TLM, and a schematic illustration of the top view of the samples used for the TLM measurements (III, inset). G1, G2, G3, and G4 samples correspond to lightly doped, moderately

https://doi.org/10.1016/j.solmat.2024.112771.

doped, and heavily doped poly-Si, and the bi-layer structure of P-doped poly-Si, respectively.

In the final evaluation of device-level performance on the M10 wafer, TOPCon solar cells were fabricated on the production line using passivation layers based on the G3 and G4 groups. The results of the electrical parameters obtained from these devices are presented in Fig. 9. The variation in V_{OC} was consistent with the independent iV_{OC} measurements. Notably, compared to the G3 group, the G4 group exhibited the highest V_{OC} value, reaching 715 mV, which could be attributed to its effective blocking of P diffusion into *c*-Si. The short circuit current density (J_{SC}) value remained constant, indicating that the incorporation of the bi-layer structure did not result in additional optical absorption losses. However, the average fill factor (*FF*) experienced a very slight decrease from 82.34% to 82.19%. This is primarily attributed to the restricted diffusion of P atoms into the substrate, leading to sub-optimal metallization contact performance. The most significant observation was the enhancement in the conversion efficiency (η), which improved from 23.58% to 23.85%, mainly due to the increase in V_{OC}. These results demonstrated that the introduction of the bi-layer structure could simultaneously enhance the electrical properties of TOPCon solar cells without any observation of film blistering.

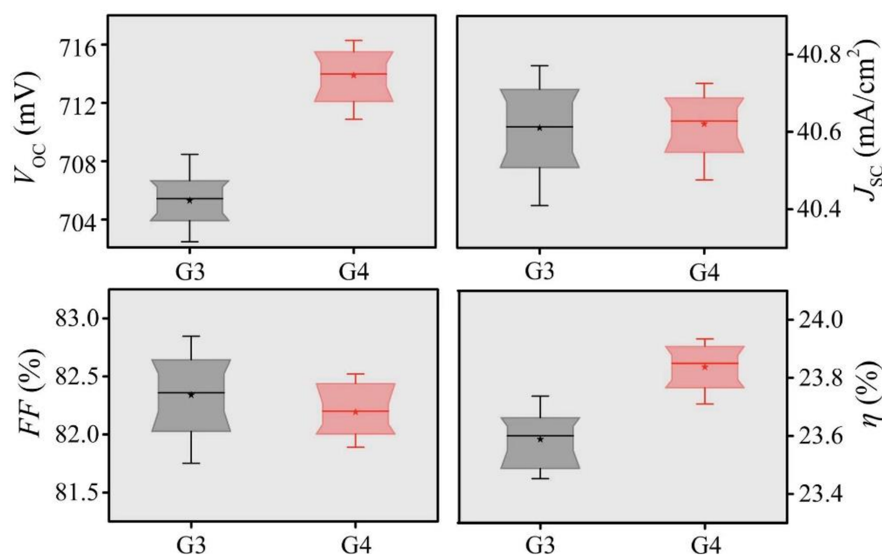

Fig. 9. Comparison of measured *J-V* parameters of TOPCon solar cells fabricated on the manufacturing line, with the use of different P-doped poly-Si films based on the G3 and G4 sample structures.

4. Conclusions

In summary, our experimental results have shown that the proposed bi-layer structure of in-situ P-doped poly-Si via the tube-PECVD approach could effectively suppress blistering while also maintain high electrical conductivity and thus simultaneously improve cell performance, which provided a simple, effective, and industrially viable method to fabricate the poly-Si required by TOPCon applications. The underlying mechanisms have been studied in detail. XPS spectra verified that more P atoms were incorporated into the poly-Si film with an increased PH_3 flow rate up to a certain threshold. From optical properties measurements by spectroscopic ellipsometry, we concluded that the parasitic absorption within the poly-Si film decreased in correlation with the

https://doi.org/10.1016/j.solmat.2024.112771.

increase of P-doping concentration. XRD spectra revealed that P-doping contributed to the enhancement in crystalline fractions of poly-Si after annealing, in alignment with subsequent observations by Raman spectroscopy. Surface morphology analyses established the efficacy of P-doped poly-Si in suppressing film blistering, which was eliminated above a certain threshold of P-doping concentration. A mechanistic exploration into the blistering mechanisms revealed that in-situ P-doping attenuated the hydrogen release and mitigated the accumulation of residual stress during annealing, thereby contributing to the blistering-free appearance of the P-doped poly-Si films. With the understanding gained, we proposed a bi-layer structure of P-doped poly-Si, which allowed us to strategically tailor the doping profile within the poly-Si film to optimize passivating contacts. Surface morphology examinations showed a blistering-free surface for the sample with the bi-layer structure, while passivation and contact resistivity tests verified the optimal electrical properties associated with the bi-layer structure. Finally, industrial-sized TOPCon solar cells were fabricated based on the bi-layer structure, achieving an average conversion efficiency of 23.84%, which was 0.26% higher than that for a TOPCon cell containing heavily P-doped poly-Si (23.58%). The above results demonstrated that the proposed bi-layer structure design for PECVD growth of in-situ P-doped poly-Si films could address the blistering bottlenecks faced by PECVD approach and has tremendous potential in industrial manufacturing. Moreover, with higher deposition rates and reduced usage of equipment-related consumables, the tube-PECVD could provide an attractive alternative route to the traditional LPCVD approach in TOPCon solar cell fabrication.

Acknowledgments

This work was supported by the Major State Basic Research Development Program of China (Grant No. 2020YFB1505502), the National Natural Science Foundation of China (Nos. 11974242, 11834011 and 52202276), and the Inner Mongolia Science and Technology Project (Grant No. 2022JBGS0036). B. L. acknowledges the funding support from the Jiangsu Specially-Appointed Professor program (Grant No. 06210061007) and the Research Funding for High-level Talents of Nantong University (No. 03083035).

References

[1] F. Feldmann, M. Bivour, C. Reichel, H. Steinkemper, M. Hermle, S.W. Glunz, Tunnel oxide passivated contacts as an alternative to partial rear contacts, Sol. Energy Mater. Sol. Cells 131 (2014) 46-50.

[2] S.W. Glunz, M. Hermle, C. Reichel, M. Bivour, F. Feldmann, A passivated rear contact for high-efficiency n-type Si solar cells enabling high V_{OC}'s and FF>82 %, in 28th European Photovoltaic Solar Energy Conference and Exhibition (2013) 988-992.

[3] J. Schmidt, R. Peibst, R. Brendel, Surface passivation of crystalline silicon solar cells: present and future, Sol. Energy Mater. Sol. Cells 187 (2018) 39-54.

[4] A.G. Aberle, S.W. Glunz, A.W. Stephens, M.A. Green, High-efficiency Silicon solar cell: Si/SiO2 interface parameters and their Impact on Device Performance, Prog. Photovoltaics Res. Appl 2 (1994) 265-273.

[5] J. Sheng, Z. Ma, W. Cai, Z. Ma, J. Ding, N. Yuan, C. Zhang, Impact of phosphorus diffusion on n-type poly-Si based passivated contact silicon solar cells, Sol. Energy Mater. Sol. Cells 203 (2019) 110120.

https://doi.org/10.1016/j.solmat.2024.112771.

[6] H. Park, H. Park, S.J. Park, S. Bae, H. Kim, J.W. Yang, J.Y. Hyun, C.H. Lee, S. H. Shin, Y. Kang, H.-S. Lee, D. Kim, Passivation quality control in poly-Si/SiO_x/*c*-Si passivated contact solar cells with 734 mV implied open circuit voltage, Sol. Energy Mater. Sol. Cells 189 (2019) 21-26.
[7] A. Richter, J. Benick, F. Feldmann, A. Fell, M. Hermle, S.W. Glunz, n-type Si solar cells with passivating electron contact: identifying sources for efficiency limitations by wafer thickness and resistivity variation, Sol. Energy Mater. Sol. Cells 173 (2017) 96-105.
[8] A. Richter, R. Müller, J. Benick, F. Feldmann, B. Steinhauser, C. Reichel, A. Fell, M. Bivour, M. Hermle, S.W. Glunz, Design rules for high-efficiency both-sides-contacted silicon solar cells with balanced charge carrier transport and recombination losses, Nat. Energy 6 (2021) 429-438.
[9] F. Haase, C. Hollemann, S. Schäfer, A. Merkle, M Rienäcker, J. Krügener, R. Brendel, R. Peibst, Laser contact openings for local poly-Si-metal contacts enabling 26.1%-efficient POLO-IBC solar cells, Sol. Energy Mater. Sol. Cells 186 (2018) 184-193.
[10] L. Wei, Y. Shi, F.G. Peng, M. Yang, L. Fang, X.N. Ru, M.H. Qu, H.F. Lin, X. Xu, On the limiting efficiency for silicon heterojunction solar cells, Sol. Energy Mater. Sol. Cells 231 (2021) 111291.
[11] F. Feldmann, R. Müller, C. Reichel, M. Hermle, Ion implantation into amorphous Si layers to form carrier-selective contacts for Si solar cells, Phys Status Solidi-Rapid Res Lett 8(9) (2014) 767-770.
[12] C. Reichel, F. Feldmann, R. Müller, R.C. Reedy, B.G. Lee, D.L. Young, P. Stradins, M. Hermle, S.W. Glunz, Tunnel oxide passivated contacts formed by ion implantation for applications in silicon solar cells, J Appl Phys 118(20) (2015) 205701.
[13] G. Nogay, J. Stuckelberger, P. Wyss, Q. Jeangros, C. Allebé, X. Niquille, F. Debrot, M. Despeisse, F-J. Haug, P. Loper, C. Ballif, Silicon-rich silicon carbide hole-selective rear contacts for crystalline-silicon-based solar cells, ACS Appl Mater Interfaces 8(51) (2016) 35660-35667.
[14] J. Stuckelberger, G. Nogay, P. Wyss P, M. Lehmann, C. Ballif, Passivating electron contact based on highly crystalline nanostructured silicon oxide layers for silicon solar cells, Sol. Energy Mater. Sol. Cells 158 (2016) 2-10.
[15] J. Kang, W. Liu, T. Allen, B. M.D. Bastiani, X. Yang, S.D. Wolf, Intrinsic silicon buffer layer improves hole-collecting poly-Si passivating contact, Adv Mater Interfaces 7(13) (2020) 2000188.
[16] K.C. Fong, T. C. Kho, W.S. Liang, T. K. Chong, M. Ernst, D. Walter, M. Stocks, E. Franklin, K. McIntosh, A. Blakers, Phosphorus diffused LPCVD polysilicon passivated contacts with in-situ low-pressure oxidation, Sol. Energy Mater. Sol. Cells 186 (2018) 236-242.
[17] M.K. Stodolny, J. Anker, C.J.J. Tool, M. Koppes, I.G. Romijn, Novel schemes of P+ poly-Si hydrogenation implemented in industrial 600 bifacial front-and-rear passivating contacts solar cells, In: 35th European Photovoltaic Solar Energy Conference and Exhibition. International Conference EU PVSEC for Photovoltaic Research (2018) 414-417.
[18] S. Duttagupta, N. Nandakumar, P. Padhamnath, J.K. Buatis, R. Stangl, A.G. Aberle, monoPoly™ cells: large-area crystalline silicon solar cells with fire-through screen printed contact to doped polysilicon surfaces, Sol. Energy Mater. Sol. Cells 187 (2018) 76-81.
[19] G. Limodio, G. Yang, Y.D. Groot, P. Procel, M. Zeman, Implantation-based passivating contacts for crystalline silicon front/rear contacted solar cells, Prog Photovoltaics Res Appl 28(5) (2020) 403-416.
[20] A. Merkle, S. Seren, H. Knauss, B. Min, J. Steffens, B. Terheiden, R. Brendel, R. Peibst,

https://doi.org/10.1016/j.solmat.2024.112771.

Atmospheric pressure chemical vapor deposition of in-situ doped amorphous silicon layers for passivating contacts, In: 35th European Photovoltaic Solar Energy Conference and Exhibition. EU PVSEC (2018) 785-791.
[21] S. Li, M. Pomaska, J. Hoss, J Lossen, F. Pennartz, M. Nuys, R. Hong, A. Schmalen. J. Wolff, F. Finger, Poly-Si/SiO_x/*c*-Si passivating contact with 738 MV implied open circuit voltage fabricated by hot-wire chemical vapor deposition, Appl Phys Lett 114(15) (2019) 153901.
[22] D. Yan, A. Cuevas, S.P. Phang, Y. Wan, D. Macdonald, 23% efficient p-type crystalline silicon solar cells with hole-selective passivating contacts based on physical vapor deposition of doped silicon films, Appl Phys Lett 113(6) (2018) 061603.
[23] J. Ho, J. Baumann, M. Berendt, U. Graupner, R. Khler, J. Lossen, M. Thumsch, E. Schneiderlchner, Sputtering of silicon thin films for passivated contacts, In: AIP Conference Proceedings, AIP Publishing LLC (2019) 40007.
[24] J. Steffens, J. Rinder, G. Hahn, Compensation of the sputter damage during A-Si deposition for poly-Si/SiO_x passivating contacts by ex-situ P-doping, In: AIP Conference Proceedings, AIP Publishing LLC (2019) 40018.
[25] L. David, S. Hübner, B. Min, C. Hollemann, T. Dippell, P. Wohlfart, R. Peibst, R. Brendel, Fired-only passivating poly-Si on oxide contacts with DC-sputtered in-situ phosphorous-doped silicon layers, In: 37th European Photovoltaic Solar Energy Conference and Exhibition, EU PVSEC (2020) 184-187.
[26] D. Yan, A. Cuevas, J. I. Michel, C. Zhang, Y. Wan, X. Zhang, J. Bullock, Polysilicon passivated junctions: The next technology for silicon solar cells? Joule 5 (2021) 811-828.
[27] S. Ma, B. Liao, F.Y. Qiao, D. Ding, C. Gao, Z.P. Li, R. Tong, X.Y. Kong, W. Z. Shen, 24.7% industrial tunnel oxide passivated contact solar cells prepared through tube PECVD integrating with plasma-assisted oxygen oxidation and in-situ doped polysilicon, Sol. Energy Mater. Sol. Cells 257 (2023) 112396.
[28] Q. Yang, M. Liao, Z. Wang, J. Zheng, Y. Lin, X. Guo, Z. Rui, D. Huang, L. Lu, M. Feng, P. Cheng, C. Shou, Y. Zeng, B. Yan, J. Ye, In-situ phosphorus-doped polysilicon prepared using rapid-thermal anneal (RTA) and its application for polysilicon passivated-contact solar cells, Sol. Energy Mater. Sol. Cells 210 (2020) 110518.
[29] B. Nemeth, D. L. Young, M. R. Page, V. Lasalvia, S. Johnston, R. Reedy, P. Stradins, polycrystalline silicon passivated tunneling contacts for high-efficiency silicon solar cells, J. Mater. Res 31(2016) 671-681.
[30] W. Duan, Y. Qiu, L. Zhang, J. Yu, J. Bian, Z. Liu, Influence of precursor a-Si dehydrogenation on the aluminum-induced crystallization process, Mater. Chem. Phys 146 (2014) 141-145.
[31] M. Stohr, J. Aprojanz, R. Brendel, T. Dullweber, Firing-Stable PECVD SiO_xN_y/*n*-Poly-Si Surface Passivation for Silicon Solar Cells, ACS Appl. Energy Mater 4 (2021) 4646-4653.
[32] S. Choi, O. Kwon, K.H. Min, M.S. Jeong, K.T. Jeong, M.G. Kang, S. Park, K.K. Hong, H.E. Song, K.H. Kim, Formation and Suppression of Hydrogen Blisters in Tunnelling Oxide Passivating Contact for Crystalline Silicon Solar Cells, Sci. Rep 10 (2020) 9672.
[33] A. Morisset, R. Cabal, B. Grange, C. Marchat, J. Alvarez, M.E. Gueunier-Farret, S. Dubois, J.P. Kleider, Highly Passivating and Blister-Free Hole Selective Poly-Silicon Based Contact for Large Area Crystalline Silicon Solar Cells, Sol. Energy Mater. Sol. Cells 200 (2019) 109912.
[34] D. Yan, S.P. Phang, Y. Wan, C. Samundsett, D. Macdonald, A. Cuevas, High-Efficiency N-Type

https://doi.org/10.1016/j.solmat.2024.112771.

Silicon Solar Cells with Passivating Contacts Based on PECVD Silicon Films Doped by Phosphorus Diffusion, Sol. Energy Mater. Sol. Cells 193 (2019) 80-84.
[35] A. Morisset, R. Cabal, B. Grange, C. Marchat, J. Alvarez, M.E. Gueunier-Farret, S. Dubois, J.P. Kleider, Conductivity and surface passivation properties of boron-doped poly-silicon passivated contacts for *c*-Si solar cells, Phys. Status Solidi A 216 (2018) 1800603.
[36] Y.R. Lin, Z.H. Yang, Z.K. Liu, J.M. Zheng, M.M. Feng, Y.Y. Zhi, L.N. Lu, M.D. Liao, W. Liu, D. Ma, Q.L. Han, H. Cheng, Q.S. Zeng, Z.Z. Yuan, B.J. Yan, Y.H. Zeng, J.H. Ye, Dual-functional carbon-doped polysilicon films for passivating contact solar cells: regulating physical contacts while promoting photoelectrical properties, Energy Environ. Sci 14 (2021) 6406-6418.
[37] Q. Yang, Z.K. Liu, Y.R. Lin, W. Liu, M.D. Liao, M.M. Feng, Y.Y. Zhi, J.M. Zheng, L.N. Lu, D. Ma, Q.L. Han, H. Cheng, Z.H. Yang, K. Ding, W. Duan, H. Chen, Y. Wang, B.J. Yan, Y.H. Zeng, J.H. Ye, Passivating Contact with Phosphorus-Doped Polycrystalline Silicon-Nitride with an Excellent Implied Open-Circuit Voltage of 745 MV and Its Application in 23.88% Efficiency TOPCon Solar Cells, Solar RRL 5 (2021) 2100644.
[38] J.K. Zhou, X.L. Su, Q. Huang, Y.H. Zeng, D. Ma, W. Liu, B.J. Yan, J.C. Ye, J. Yang, X.Y. Zhang, H. Jin, Y. Zhao, G.F. Hou, Approaching 23% efficient n-type crystalline silicon solar cells with a silicon oxide-based highly transparent passivating contact, Nano Energy 98 (2022) 107319.
[39] R. Sharma, A. Alleva, A. Hajjiah, H.S. Radhakrishnan, J. Poortmans, Comparison of C-, N-, and O-Incorporated Non-blistering PECVD Si Films for Application in SiO_x-Based Passivating Contacts for Si Solar Cells, ACS Appl. Energy Mater 5 (2022) 9994-10001.
[40] R.A. Sinton, A. Cuevas, Contactless determination of current-voltage characteristics and minority-carrier lifetimes in semiconductors from quasi-steady-state photoconductance data, Appl. Phys. Lett 69 (1996) 2510-2512.
[41] D.E. Kane, R.M. Swanson, Measurement of the emitter saturation current by a contactless photoconductivity decay method, in: In 18th IEEE PVSC (1985) 578-583.
[42] M. Lee, S. Kim, D. Ko, Chemical state analysis of heavily phosphorus-doped epitaxial silicon films grown on Si (100) by X-ray photoelectron spectroscopy, Appl. Surf. Sci 443 (2018) 131-137.
[43] D. Briggs, M.P. Seah, Practical Surface Analysis-by Auger and X-ray Photoelectron Spectroscopy, 1983.
[44] J. Chastain, R.C. King, J. Moulder, Handbook of X-ray photoelectron spectroscopy, Physical Electronics Division, Perkin-Elmer Corporation Eden Prairie (1992) Minnesota.
[45] C.J. Powell, Elemental binding energies for X-ray photoelectron spectroscopy, Appl. Surf. Sci 89 (1995) 141-149.
[46] G.G. Wepfer, T.C. Collins, R.N. Euwema, Calculated spin-orbit splittings of some group IV, III-V, and II-VI semiconductors, Phys. Rev. B 4 (1971) 1296-1306.
[47] H.-Y. Ryu, M. Lee, H. Park, D.-H. Ko, Chemical bonding states and dopant redistribution of heavily phosphorus-doped epitaxial silicon films: Effects of millisecond laser annealing and doping concentration, Applied Surface Science 504 (2020) 144447.
[48] K.J. Chen, A. Bothwell, H. Guthrey, M.B. Hartenstein, J.-I. Polzin, F. Feldmann, W. Nemeth, S. Theingi, M. Page, D. L. Young, P. Stradins, S. Agarwal, Measurement of poly-Si film thickness on textured surfaces by X-ray diffraction in poly-Si/SiO_x passivating contacts for monocrystalline Si solar cells, Sol. Energy Mater. Sol. Cells 236 (2022) 111510.
[49] A.S. Kale, W. Nemeth, H. Guthrey, S.U. Nanayakkara, V. LaSalvia, S. Theingi, D. Findley, M.

Page, M. Al-Jassim, D.L. Young, P. Stradins, S. Agarwal, Effect of crystallographic orientation and nanoscale surface morphology on poly-Si/SiO_x contacts for silicon solar cells, ACS Appl. Mater. Interfaces 11 (2019) 42021-42031.
[50] B. Birouk, D. Madi, Thermal oxidation effect on structural and optical properties of heavily doped phosphorus polycrystalline silicon films, Appl. Phys. A104 (2011) 739-748.
[51] P. Zaumseil, High-resolution characterization of the forbidden Si 200 and Si 222 reflections (in eng), J. Appl. Crystallogr. 48 (Pt 2) (2015) 528-532.
[52] G. Nogay, J. Stuckelberger, P. Wyss, Interplay of annealing temperature and doping in hole selective rear contacts based on silicon-rich silicon-carbide thin films, Sol. Energy Mater. Sol. Cells 173 (2017) 18-24.
[53] E. Bustarret, M.A. Hachicha, M. Brunel, Experimental determination of the nanocrystalline volume fraction in silicon thin films from Raman spectroscopy, Appl. Phys. Lett 52 (1988) 1675-1677.
[54] Y. Kang, Q. Yu, Z. Lei, H. Ming, An application of Raman spectroscopy on the measurement of residual stress in porous silicon, Opt. Lasers Eng 43 (2005) 847-855.
[55] P. A. Fedders, D. J. Leopold, P. H. Chan, R. Borzi, and R. E. Norberg, Molecular hydrogen in a-Si:H, Phys. Rev. Lett 85 (2000) 401-404.
[56] A.A. Langford, M.L. Fleet, B.P. Nelson, W.A. Lanford, N. Maley, Infrared absorption strength and hydrogen content of hydrogenated amorphous silicon, Phys. Rev. B 45 (1992) 13367-13377.
[57] G. Lucovsky, R.J. Nemanich, J.C. Knights, Structural interpretation of the vibrational spectra of a-Si: H alloys, Phys. Rev. B 19 (1979) 2064-2073.
[58] K.H. Kim, E.V. Johnson, P.R. Cabarrocas, Evolution of microstructure and incorporation of excess hydrogen during the growth of hydrogenated polymorphous silicon at a high rate, J. Nanosci. Nanotechnol 17 (2017) 4920-4925.
[59] K. Nakada, S. Miyajima, M. Konagai, Amorphous silicon oxide passivation films for silicon heterojunction solar cells studied by hydrogen evolution, Jpn. J. Appl. Phys 53 (2014) 04ER13.

https://doi.org/10.1016/j.solmat.2024.112771.